A Combinatorial Vortex Detection and Characterization Algorithm for 2C2D PIV Data

Mathew Bussière[1,*], David S. Nobes[2], Charles Robert Koch[3]

1*: Department of Mechanical Engineering, University of Alberta, Canada, mjb11@ualberta.ca
2: Department of Mechanical Engineering, University of Alberta, Canada, david.nobes@ualberta.ca
3: Department of Mechanical Engineering, University of Alberta, Canada, bob.koch@ualberta.ca

Abstract In this study, the vortical wake conditions of water flowing past an oscillating symmetric airfoil are described with velocity vector fields obtained from particle image velocimetry (PIV) data. Vortices are identified and characterized with a combinatorial algorithm and were found to agree well with the Burgers vortex model. Velocity vector fields obtained experimentally are often accompanied by undesirable effects which are not present in numerical data. The algorithm overcomes these limitations in the data sets by making use of three separate detection methods to provide dependable vortex detection in a wide range of wake conditions.

1. Introduction

Vortices are essential flow features in a number of fluid flow applications. Vortex formation in the wake of airfoils and other streamlined bodies is important both in research and in practice. For example, numerous turbulent flow regimes are dominated by temporally evolving, spatially coherent structures which are generally regarded as vortices [1].

The study of flow around a pitching airfoil is useful for understanding undesirable effects such as wing flutter [2] and more recently, for understanding biologically inspired aquatic propulsion [3], [4]. In this study a NACA 0012 airfoil submersed in a vertically aligned uniform flow field, is forced to oscillate sinusoidally about its aerodynamic center which is roughly the quarter chord distance. For the flow velocities tested, the wake downstream of the airfoil is comprised of coherent structures which separate from the trailing edge of the airfoil and travel downstream at a given drift velocity. For this type of flow, accurate detection and characterization of the coherent structures in the wake is a central focus for previous research [2], [5], [6]. For a given Reynolds number, it is possible to generate several different wake schemes which are described by vortex position and organization in the wake [3].

The classification of the vortex populated wake is usually summarized using a phase diagram that maps the important wake transitions as a function of two independent dimensionless parameters. These are the Strouhal number based on the flapping frequency and dimensionless amplitude based on chord length [7], [3]. To generate these phase diagrams a reliable and accurate identification of the vortices in the wake is required. In addition to reliably detecting vortices, it is important to be able to compute several parameters that are used to describe the flow by aerodynamicists. In particular these include vortex core coordinates, vortex drift velocity, maximum vorticity, circulation, boundary radius and maximum circumferential velocity [8].

Approaches for vortex detection are often developed and tested on data obtained through direct numerical simulation (DNS) [9], [10]. Performing vortex detection on PIV data can be more difficult because of measurement noise and experimental uncertainty in the data [11]. Measurement noise is usually attenuated by filtering prior to running a detection algorithm [8] but, thresholds must be carefully selected as not to overlook weak or small vortices [11]. In addition, the flow field near the centre of the vortex experiences substantial gradients which can lead to seeding issues and

poor correlation in the PIV data [8]. While DNS data can employ local mesh refinement [12] to increase the spatial resolution in specific locations such as the vortex core, PIV detection algorithms must find other ways to overcome the sharp gradients near the core. Often, due to camera resolution, PIV data must be collected using a number of independent cameras which results in images that need to be de-warped and stitched together. This can introduce discontinuities in the flow-field image. Such discontinuities could contribute to elevated local vorticity which could be falsely identified as a vortex [1]. PIV data is becoming increasingly available by experimentalists [8] and consequently, robust vortex detection and characterization algorithms that are specifically tailored for PIV data is an important topic in modern experimental fluid mechanics.

In this paper a vortex detection algorithm has been developed by combining selected features from 3 individual algorithms. The algorithm must efficiently analyze the data and successfully detect and locate vortices as well as calculate characteristic vortex parameters. It is also essential to automatically diagnoses and detect a false positive vortex without human intervention. This paper explores the effectiveness of the proposed algorithm by studying the vortices in the well documented wake of a pitching symmetric airfoil [2], [7].

1.1 Approaches to Vortex Detection

A precise definition of a vortex does not exist [1] and this makes them difficult to detect in practical flows. The most straightforward and widespread definition of a vortex is merely the perception of swirling movement of fluid about a central point [9]. It is difficult to translate such an intuitive notion, which is based on human perception, into a strict numerical characterization which can be detected by numerically driven algorithms.

Lugt (1979) suggested that "*A vortex is the rotating motion of a multitude of material particles around a common center"*. This is consistent with the earlier definition however it does not introduce any new criteria for characterizing vortical structures, nor does it provide a valuable definition from which a vortex detection algorithm can be developed. Building upon the former definition, Robinson (1991) proposes that "*A vortex exists when instantaneous streamlines mapped onto a plane normal to the vortex core exhibit a roughly circular or spiral pattern, when viewed from a reference frame moving with the center of the vortex core"*. This definition provides a precise geometric characterization however, detection of a vortex using this approach requires *a priori* information about the location of its core, making it difficult to implement a sensible systematic vortex detection procedure. It can, however, be a useful basis for developing an automated vortex verification algorithm. Jeong & Hussain (2006) also suggest that *"A vortex core must have a net vorticity, hence net circulation"*. This provides an instant means for identifying regions where vortices may reside without any previous knowledge of the location or drift velocity of a vortex core. Scalar vorticity fields are easily computed from the velocity vectors and regions of interest can then be generated and labeled. This definition combined with the definition of Robinson (1991) is a sensible foundation for developing a robust vortex detection algorithm.

Vortex detection methods are often carefully tailored to work with specific data types and specific flow-fields. As a result, they are tuned to detect precise structures based on unambiguous definitions of the vortices of interest [9]. The algorithms can be quite sensitive to parameters such as vortex spacing, should there be multiple vortices in a given flow-field, vortex size, angular velocity and the presence of shear flow [8].

Ari Sadarjoen (2000) suggests that the various vortex detection algorithms reported in the literature can be divided into two distinct groups. The first is a more traditional class of vortex detection algorithms based on evaluating physical quantities of the flow-field at specific points. Common parameters to measure are velocity, vorticity, pressure and the velocity gradient tensor. Ari Sadarjoen (2000) stressed that a major shortcoming of this class is that the algorithms are less sensitive to large, slow rotating vortices. For example, the maximum vorticity method [9] defines a

vortex core as a local maximum of vorticity magnitude. This method inherently ignores regions where the vorticity falls below a defined threshold and will likely fail to detect weak, slow rotating vortices.

A second group based on geometric methods represents a relatively new set of vortex detection algorithms. These algorithms rely on geometric features, such as streamlines and pathlines, rather than scalar properties evaluated at individual grid points [9]. While being more computationally demanding, they make up for a common deficiency in traditional methods with their ability to automatically distinguish false positives from actual vortices [9], [14].

2. Development of a vortex detection algorithm

The basic concepts and approaches to vortex detection that can be used in developing an algorithm can be explored by reviewing three vortex detection methods that have been used in the literature. These are the maximum vorticity (MV) method [15], the cross sectional lines (CSL) method (Vollmers 2001) and the winding angle (WA) method [16]. The following section discusses the main aspects of each which will be used to develop a combinatorial vortex detection (CVD) method for use on PIV data.

2.1 Maximum vorticity (MV) method

Strawn et al. (1999) proposed that a vortex core exists where there is a local maximum of vorticity magnitude. Maximum vorticity successfully identifies vortices in close proximity, where the cores may be overlapping [9]. However, a major drawback to this method is that vorticity does not only identify vortices, it also identifies regions where shearing activity occurs [1]. This makes it more challenging to develop a vortex detection algorithm based solely on vorticity fields for non free-shear flow regimes [1], [9]. Alternatively, vorticity fields can provide a means of outlining a region-of-interest (ROI) where potential vortices might be located, and other algorithms will be used to evaluate these ROI individually.

For the CVD, a Gaussian low pass spatial filter was applied to the velocity data to produce a smooth field and eliminate any small scale fluctuations which could cause local spikes in the vorticity field. Scalar vorticity ω, computed numerically at every grid point, is defined in the two-dimensional velocity field $\vec{v}$ by:

$$\omega = \vec{\nabla}\times\vec{v} \tag{1}$$

In order to detect weak vortices with relatively low vorticity, a low vorticity threshold must be applied; however, this runs the risk of lumping stronger, closely spaced vortices into one single ROI where it would be evaluated as a single vortex structure. To circumvent this, multilevel thresholds are used and the resulting indexed image is analyzed with logical operators and image morphology (IM) techniques.

A multilevel threshold is applied with the intention that weak vortices may be identified without preventing the ability to distinguish strong vortices with overlapping cores or that are simply in close proximity. Figure 1illustrates two test case vorticity fields and how a 3 level threshold can be applied. The resulting indexed image along with a desired ROI map is shown for the two sample vorticity fields. The images in the left column of Figure 1 are the resulting indexed images where i=1,2,3 while the right column represents the desired ROI map that is to be extracted from the corresponding indexed image. Without a multilevel threshold, only one of the three threshold levels would be used and would lead to one of the following scenarios:

- When only threshold level 1 is used: The larger region, which clearly has two distinct peaks of vorticity, is lumped into one single ROI and is treated as a single potential vortex. However, this region has 2 distinct peaks and should be treated as 2 individual ROIs.
- When only threshold level 3 is used: The weaker vortices, do not meet the vorticity ω_{peak} level 3 threshold, are not considered to be ROIs and are not identified as potential vortices.

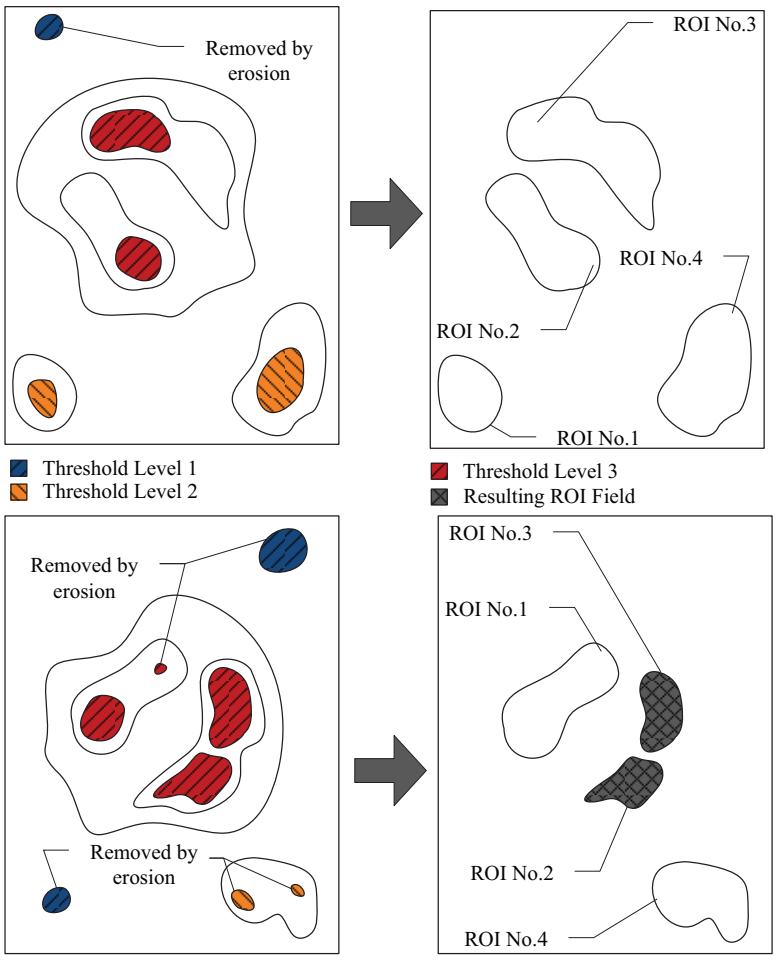

Figure 1:Result of multilevel threshold technique for two different cases on a supposed vorticity map

To overcome some of these major limitations of using a single level threshold to identify ROIs, an ROI map is generated with the algorithm outlined in Figure 2The proposed algorithm thresholds the vorticity field returning an indexed image using the threshold values defined by the threshold intensity vector (*TIV*):

$$TIV = \langle TI_1, TI_2, TI_3 \rangle \quad (2)$$

Morphological opening is performed for each of the thresholds defined in *eqn.* 2. It is a process which combines 2 basic image morphology techniques, erosion and dilation, and executes them in a specific order. First, the image is eroded with a diamond shaped structuring element of size S_e. Clusters of pixels smaller than S_e are removed and those larger than size S_e are made smaller. Then dilation is performed with the same structuring element S_e to restore the clusters of pixels that were not removed by erosion to their original size.

Groups of connected pixels formed by index I_1 are first morphologically opened with an IM

diamond shaped structuring element of size S_{e1} then they are labeled and investigated individually. Structures from index I_2 are first morphologically opened with an IM diamond shaped structuring element of size S_{e2}, then sub-labeled within each of the labeled groups from index I_1. If no groups from index I_2 are contained within a given group from index I_1 then the algorithm terminates and the group of pixels from index I_1 becomes a ROI. However, if at least one group from index I_2 is detected within a given index I_1 group, then pixels from index I_3 are morphologically opened with an IM diamond shaped structuring element of size S_{e3}, and subsequently sub-labeled within each of the index I_2 groups. At this point the algorithm counts the number of groups at each level. If multiple index I_3 groups are detected within an index I_2 cluster, then each individual index I_3 group forms a ROI. If only one index I_3 group is counted, then the algorithm falls back a level and considers the number of index I_2 clusters. Again, if multiple index I_2 groups are detected then each individual index I_2 group forms a ROI and, if only one index I_2 label is detected, the index I_1 group becomes the ROI. In this manner, the ROIs will always consider the largest possible area, but will separate into multiple ROIs when multiple distinct, higher vorticity peaks are detected.

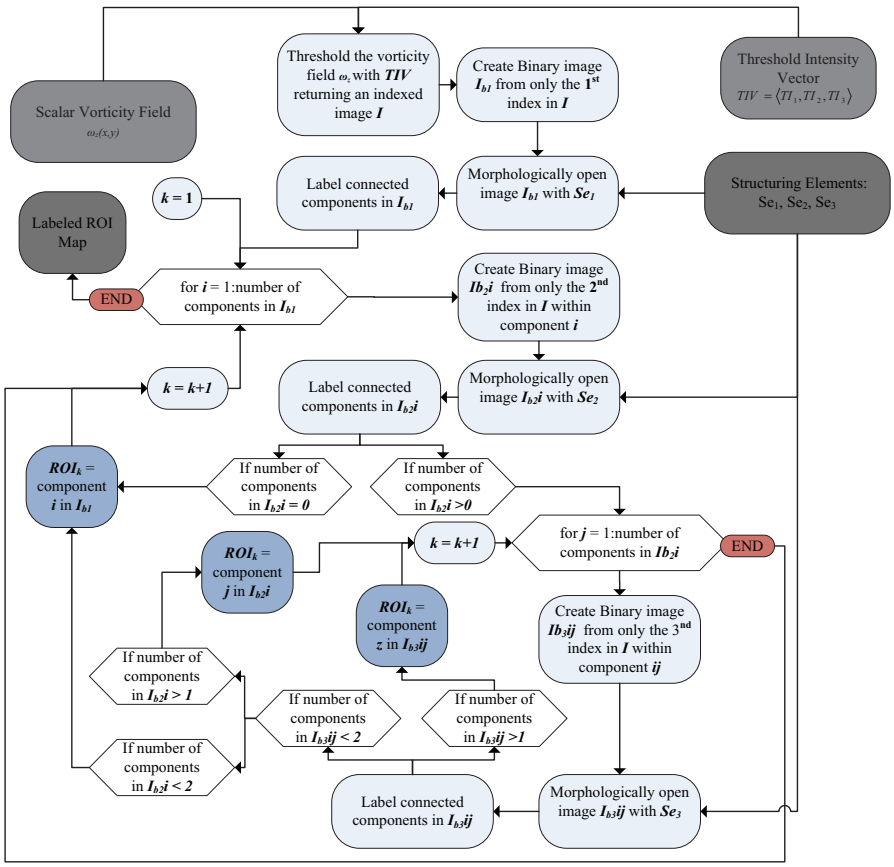

Figure 2: Multilevel threshold and image morphology algorithm schematic

2.2 Cross sectional lines (CSL) method

This method locates a potential vortex core in a given ROI by measuring the velocity component perpendicular to parallel straight cross sectional lines (CSLs) cutting the ROI at an arbitrary angle [8]. The CSL method is implemented and inspected for its ability to accurately and consistently locate vortex cores in ROIs which were identified and labeled with the MV algorithm. It is important to recognize that the CLS method does not detect vortices. It merely locates potential

vortex cores and boundary radii. The method will output the two dimensional coordinates of a core whether or not a vortex actually exists in the current ROI.

A CSL algorithm similar to the one described by [17] is performed for each of the labeled ROI. A schematic outlining the essential CSL procedure is shown in Figure 3 where a sample vortex is shown. The concentric circles represent vorticity contours and the core is shown as a red '×'.

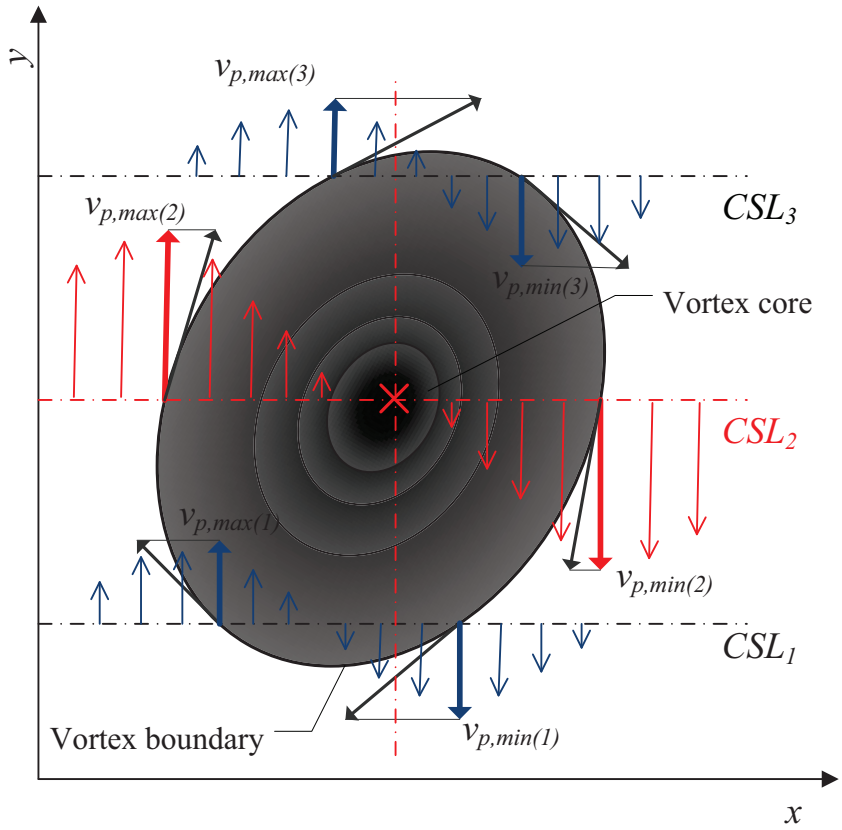

Figure 3: Cross sectional lines procedure schematic

For an $A \times B$ vector velocity field, the y-component of velocity $v_{y(i,j)}$ is evaluated for columns $i = 1,2,3 \ldots A$ and rows $j = 1,2,3 \ldots B$ along every row in each of the ROIs. When discussing the CSL method, velocity $v_{y(i,j)}$ is referred to as the perpendicular velocity $v_{p(i,j)}$. The maximum and minimum perpendicular velocities for each row j within a given ROI are defined as:

$$v_{p,\max(j)} = \max(v_{p(A_s,j)}, v_{p(A_s+1,j)}, \ldots, v_{p(A_e,j)}) \quad (3)$$

and

$$v_{p,\min(j)} = \min(v_{p(A_s,j)}, v_{p(A_s+1,j)}, \ldots, v_{p(A_e,j)}) \quad (4)$$

The indices A_s and A_e refer to the first and last velocity vectors within a ROI on a given row respectively. The row ψ within the ROI with the largest difference $|v_{p,\max(j)} - v_{p,\min(j)}|$ is referred to as the critical CSL written as CSL_ψ and it represents the y-coordinate of a vortex core, should one exist in the ROI under evaluation. The perpendicular velocity along this row is then written as $v_{p(i,\psi)}$. The x-coordinate of the vortex core is the location on CSL_ψ where the velocity is:

$$v_{p(\varsigma,\psi)} = \frac{\left(v_{p,\max(\psi)} + v_{p,\min(\psi)}\right)}{2} \quad (5)$$

and the coordinates of the vortex core are then given by (ς, ψ).

For simplicity, the hypothetical vortex shown in Figure 3 only reveals 3 rows/lines of the v_y velocity field. The critical perpendicular line is $CSL_\psi = CSL_2$ and is plotted in red. A comparison with the other two lines reveals that CSL_2 has the largest difference between its maximum and minimum perpendicular velocities $v_{p,\max(2)}$ and $v_{p,\min(2)}$. Consequently, the *y*-coordinate for the hypothetical vortex core is $\psi = 2$. Evaluation of *eqn. 5* along CSL_2 gives velocity $v_{p(\varsigma,2)}$. The algorithm searches for $v_{p(\varsigma,2)}$ along CSL_2 to find ς. The two computed coordinates locate the vortex core of a potential vortex in the ROI; however it does not determine whether the ROI truly does contain a vortex. Other vortex detection methods should be used to verify that a particular ROI contains a vortex. The CSL method provides an estimation of vortex size by fitting a circle of radius r_v centered at the core with length [8]:

$$r_v = \frac{\left|\varsigma_{v,\max(\psi)} - \varsigma_{v,\min(\psi)}\right|}{2} \quad (6)$$

where, $\varsigma_{v,\max(\psi)}$ refers to the column index on row ψ where the velocity vector $v_{p,\max(\psi)}$ is located and $\varsigma_{v,\min(\psi)}$ refers to the column index on row ψ where the velocity vector $v_{p,\min(\psi)}$ is located. Finally, Vollmers (2001) proposed that the transverse and streamwise components of the drift velocity $\vec{v}_{drift} = (v_{drift,x}, v_{drift,y})$ are respectively the *x* and *y* components of velocity evaluated at the core coordinate (ς, ψ).

Geometric methods such as the winding angle method require a reference frame moving at the core velocity of a vortex. This is especially challenging when the vortices do not have similar drift velocities and different sets of streamlines must be calculated for each reference frame belonging to each of the different drift velocities. Unlike most geometric methods, the CSL method can locate stationary and dynamic vortex cores and hence, a fixed reference frame is not necessary. In short, performing CSL does not require *a priori* knowledge of the location or velocity of the vortex core; it only requires pre-defined ROI where suspect vortices are potentially located. The CSL method is ideally suited for locating vortex cores and estimating vortex size and drift velocity in flow fields where little is known about the vortical structures present. The algorithm is performed on pre-defined ROI which are computed with the MV method. The CSL algorithm used in this study is summarized in the flow chart shown in Figure 4. The algorithm is comprised of two primary nested loops; one for the individual ROI and the second for the individual CSLs in each ROI. The input (shown as grey boxes) is comprised of the 2C2D global velocity field and the labeled ROI map.

A shortcoming of the CSL method is its inherent inability to reject false positives by identifying a vortex core in a ROI which does not contain a vortex. To overcome this problem, a hybrid detection algorithm comprised of the MV, CSL and a geometric method is proposed. Since geometric methods can effectively identify and reject false positives often ignored by other methods, when combined with geometric detection method and CSL method, a more robust detection method is obtained. The proposed geometric detection method is the winding angle (WA) method.

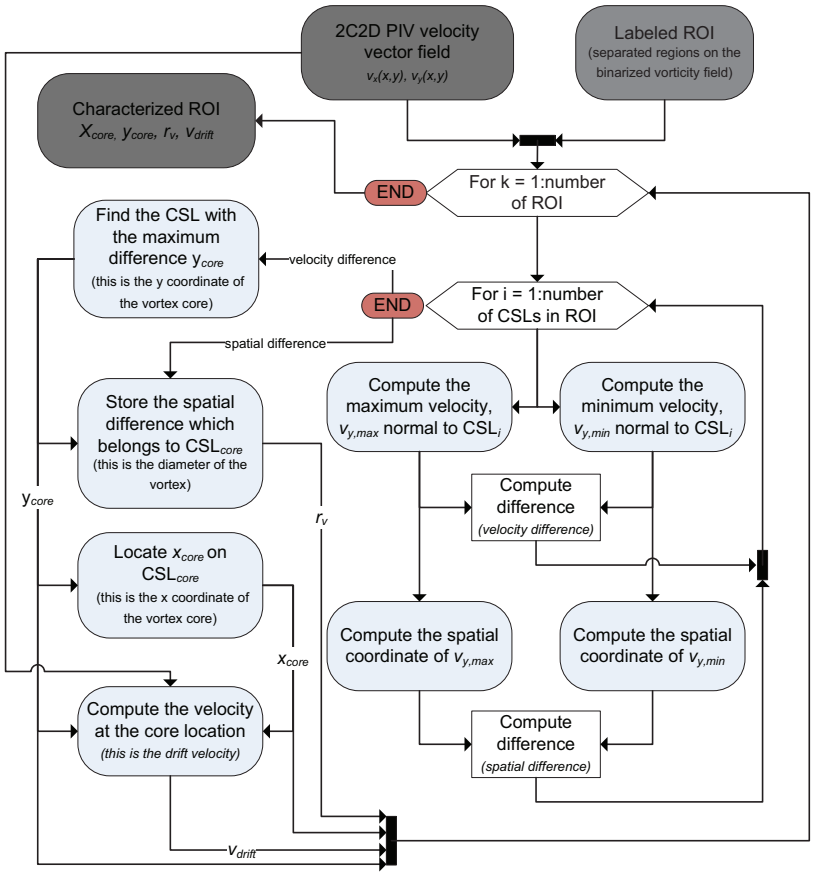

Figure 4: Cross sectional lines (CSL) algorithm flow chart

2.3 Winding angle (WA) method

The WA method, first proposed by Portela (1999), is a geometric vortex detection method which evaluates discretized streamlines and determines if they belong to a vortex. Ari Sadarjoen (2000) suggested that a streamline must satisfy two criteria to be considered part of a vortex. Firstly, the winding angle α_w along a streamline must be $\alpha_w \geq n2\pi$, where $(n = 1,2,3 \ldots)$. Here the winding angle for streamline S_k is defined as the sum of all the angles $(\angle)$ between line segments of a discretized streamline composed of N connected points P_k:

$$\alpha_{w,k} = \sum_{i=1}^{N-1} \angle\left(P_{k,i-1}, P_{k,i}, P_{k,i+1}\right) \tag{7}$$

A streamline belonging to a vortex is characterized by a closed semi elliptic path [1],[14], [18], [19] and the winding angle criterion alone is not enough to satisfy this requirement [14]. It is possible for a streamline to have a sufficiently large winding angle yet not follow a closed path; therefore, a second provision is necessary. The second criterion states that the distance between the starting and the ending point of a streamline should be reasonably small [14]. This second requirement is unfortunately qualitative since it depends on the length scale of the flow-field as well as the total length of the calculated streamlines.

Streamlines that comply with the two criteria above are then linked to a precise vortical structure. An automated process which groups all of the streamlines meeting the above criteria and tags them according to which vortex they are believed to belong to is described by Ari Sadarjoen

(2000). This is done by mapping each streamline to a cluster point and then grouping all cluster points that are in close proximity. Each cluster point is the arithmetic average of the vertices which make up a given streamline. A maximum separation determines how far apart a cluster point must be from other points before it is marked as a new group. One particular limitation of this method is the separation distance must be specified *a priory* and it depends heavily on the vortex spacing of the flow field.

This method is well suited for detection of multiple vortices given suitable starting points for streamlines and predefined ROI with local velocity vector fields [9]. The local velocity vector fields must have a reference velocity that matches the drift velocity of the core. For this reason the WA method cannot be performed on a global field since the vortices can potentially have different drift velocities [8]. As a constituent of the geometric vortex detection class, the WA method is computationally taxing [9]. However, for 2D flow fields computation time is not typically an issue. In addition, geometric methods are robust and unlike other traditional methods they can reliably distinguish false positives from true vortices [9].

The WA method searches for streamlines that form closed paths by evaluating two specific requirements. It then groups the complying streamlines according to which vortex they are believed to belong to. The first requirement is that the 2D winding angle $\alpha_{w,k}$ for streamline S_k must be $\left|\alpha_{w,k}\right| = n2\pi$ where n is a positive integer [20] The signed angle $\alpha_{k,i}$ between vectors $\overrightarrow{V_1}$and $\overrightarrow{V_2}$ on a given streamline is given by:

$$\alpha_{k,i} = \frac{\cos^{-1}\left(\overrightarrow{V_1} \cdot \overrightarrow{V_2}\right)}{\left|\overrightarrow{V_1}\right|\left|\overrightarrow{V_2}\right|}\left(\frac{\overrightarrow{V_n} \cdot \left(\overrightarrow{V_1} \times \overrightarrow{V_2}\right)}{\left|\overrightarrow{V_n} \cdot \left(\overrightarrow{V_1} \times \overrightarrow{V_2}\right)\right|}\right) \tag{8}$$

where,

$$\overrightarrow{V_1} = \langle\left(P_{x,(i-1)} - P_{x,(i-2)}\right), \left(P_{y,(i-1)} - P_{y,(i-2)}\right), 0\rangle \tag{9}$$

and

$$\overrightarrow{V_2} = \langle\left(P_{x,i} - P_{x,(i-1)}\right), \left(P_{y,i} - P_{y,(i-1)}\right), 0\rangle \tag{10}$$

and

$$\overrightarrow{V_n} = \langle 0,0,1\rangle \tag{11}$$

Here, P_x and P_y are the respective (x,y) location on a given streamline and $\overrightarrow{V_n}$ is a unit vector normal to the flow-field of interest. Figure 5 demonstrates how the individual angles $\alpha_{k,i}$ are calculated on a section from streamline S_k. Here, the angle $\alpha_{k,i}$ measured from $\overrightarrow{V_1}$to $\overrightarrow{V_2}$ is CW. By the same convention, the next angle $\alpha_{k,(i+1)}$ would be CCW positive. The winding angle $\alpha_{w,k}$ for streamline S_k is determined by summing for all points on the streamline as follows:

$$\alpha_{w,k} = \sum_{i=2}^{N} \alpha_{k,i} \tag{12}$$

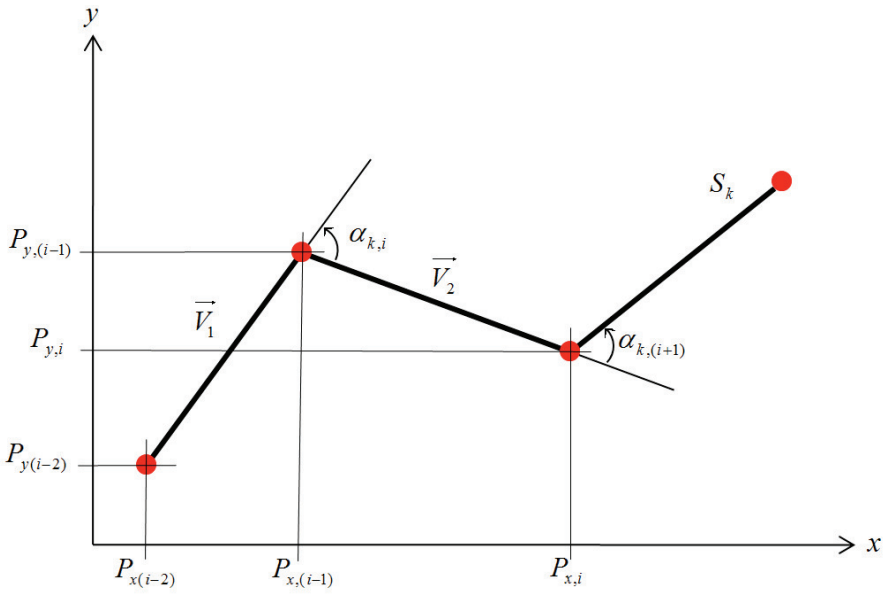

Figure 5: Computation of angle $\alpha_{k,i}$ on streamline S_k for the winding angle algorithm

The second requirement states that a streamline which is part of a vortex must have its starting and ending points relatively close together [20]. The distance between the starting ($P_{x,1}$, $P_{y,1}$) and ending point ($P_{x,N}$, $P_{y,N}$) of a streamline S_k shown in Figure 6 is given by:

$$D_{se} = \sqrt{\left(P_{x,N} - P_{x,1}\right)^2 + \left(P_{y,N} - P_{y,1}\right)^2} \tag{13}$$

The starting location of a streamline is pre-defined and each streamline is comprised of a fixed number of points and a set spacing between them. Consequently, a streamline on a closed path can start and end anywhere on the path since the length of the streamline is a predefined value. Then, the maximum distance separating the start and end points of an arbitrary streamline on a closed circular path would be equal to the diameter of the circle defining that path. This identifies a major challenge for defining a D_{se} threshold, since streamlines on larger vortices require a large D_{se}; however, too large of a D_{se} threshold could lead to non-vortical streamlines being incorrectly associated to relatively small vortices. This is remedied by splitting streamlines when the cumulative sum of angles reaches the highest multiple of 2π. In this manner, the start and end points of a streamline on a closed path will always be a minimum.

Although the WA threshold is defined as $|\alpha_{w,k}| = n2\pi$; a suitable value for the threshold D_{se} must be selected. The D_{se} threshold depends on the length scale of the vortical structures present which unfortunately requires *a priori* knowledge of the expected size and spacing of the vortices in the flow field. The ROIs defined previously can be used to define a sensible threshold for D_{se}. Circles of radius r_v are fitted to the suspected vortices in each ROI. This parameter is a sensible length scale for coherent structures in the flow field of interest. Therefore a reasonable choice for the D_{se} threshold would be some value that is larger than $r_v / 2$. This ensures that a streamline with a sufficiently large distance between its starting and ending points is not considered to be part of a vortex since its length scale would be much larger than any other structure in the current flow field.

The final task of the algorithm is to determine whether the individual streamlines conform to the specified thresholds. Streamlines that pass all the required criteria are marked and numbered. The sign of the winding angle $\alpha_{w,k}$ for each streamline determines the direction of rotation of the vortex associated to that streamline.

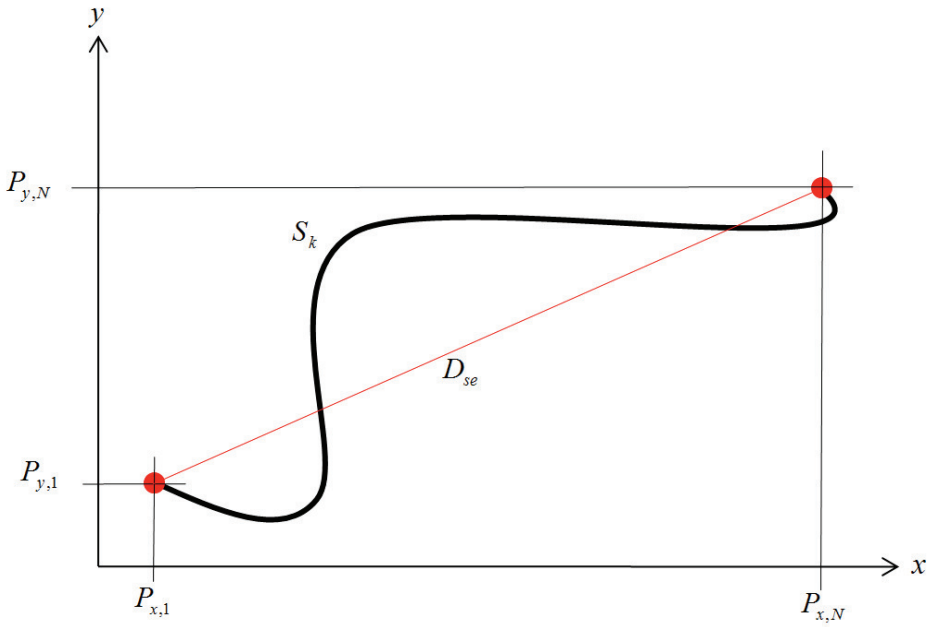

Figure 6:Computation of length D_{se} for the winding angle algorithm

It is possible for an ROI to enclose multiple vortices. If this is the case it becomes necessary to label all of the closed streamlines accordingly. This is done by first mapping each of the closed streamlines to a point, then labeling clusters of closely grouped points [20]. The vortical streamlines S_k are mapped to points MP_k in the following manner:

$$MP_{x,k} = \frac{1}{N}\sum_{i=1}^{N} P_{x,i} \tag{14}$$

and

$$MP_{y,k} = \frac{1}{N}\sum_{i=1}^{N} P_{y,i} \tag{15}$$

The distance between MP_k and some other point $MP_{k'}$ is calculated as follows:

$$D_{MP_{k,k'}} = \sqrt{\left(MP_{x,k} - MP_{x,k'}\right)^2 + \left(MP_{y,k} - MP_{y,k'}\right)^2} \tag{16}$$

The first point MP_1 defines the first cluster group. If the distance between MP_1 and MP_2 is within a prescribed tolerance, then MP_2 is labeled as group 1. If the distance exceeds the tolerance, then MP_2 defines a new group. For point MP_3, both distances $D_{MP_{3,1'}}$ and $D_{MP_{3,2}}$ are calculated. If neither value is within tolerance, then MP_3 defines a new cluster group. However, if either $D_{MP_{3,1'}}$ or $D_{MP_{3,2}}$ are within tolerance then MP_3 will belong to the closest group. All other points are labeled in this manner. Finally, once all of the streamlines are labeled, their arithmetic average is computed for each cluster group.

The WA algorithm used in this study is summarized by way of the flow chart shown in Figure 7. The algorithm is comprised of three nested loops: one investigates the ROIs, the second is for the instantaneous streamlines within each ROI and the third loop is concerned with the individual grid-points comprising each streamline. The input consists of the streamlines calculated from local velocity fields having a reference velocity equal to the drift velocity of the corresponding ROI.

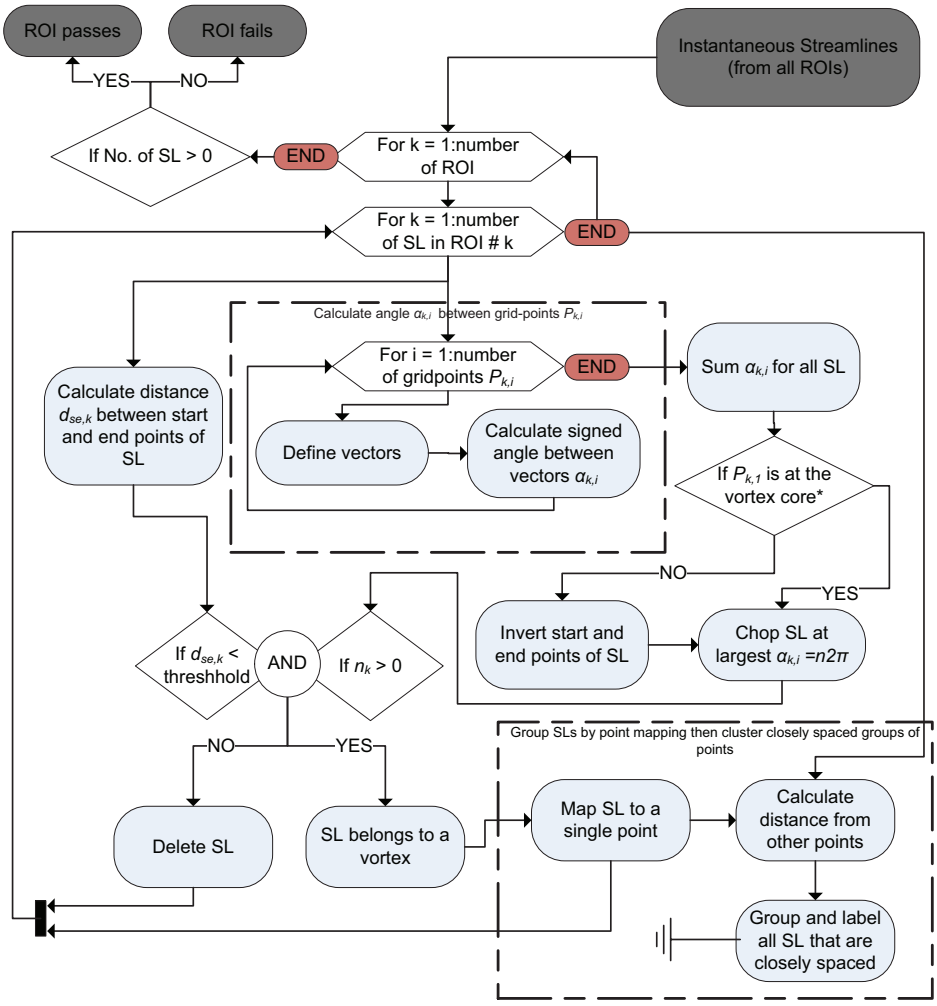

Figure 7: Winding angle algorithm flow chart

The winding angle method is particularly sensitive to the reference velocity chosen for the computation of the required streamlines and hence, does not provide accurate estimates of vortex boundary in the event that the reference velocity is not precisely that of the vortex core. While the WA method does not generally provide a good estimate of vortex size and shape, it is extremely robust when it comes to eliminating false positives [20]. The WA method serves as a means of verifying if other detection techniques are accurate. The most apparent way to determine if a detection algorithm truly locates a vortex is by visual inspection. However, this seems counter intuitive since automation is the primary value of detection algorithms. For this reason, the WA method serves as a swirling flow verification once potential vortex core location and drift velocity are computed via other detection methods.

2.4 The combinatorial vortex detection (CVD) method

The CVD method was developed using a combination of the first three detection algorithms and simple image morphology techniques. An aim in the development of the method was that it must consistently detect and characterize multiple vortices from PIV generated velocity vector maps. It must label each vortex in the flow field and locate the vortex cores, the drift velocity, the

circulation, the peak vorticity and boundary radii of the individual vortical structures. Ultimately, the method must reduce the size of the original dataset, by accurately conserving important vortex parameters.

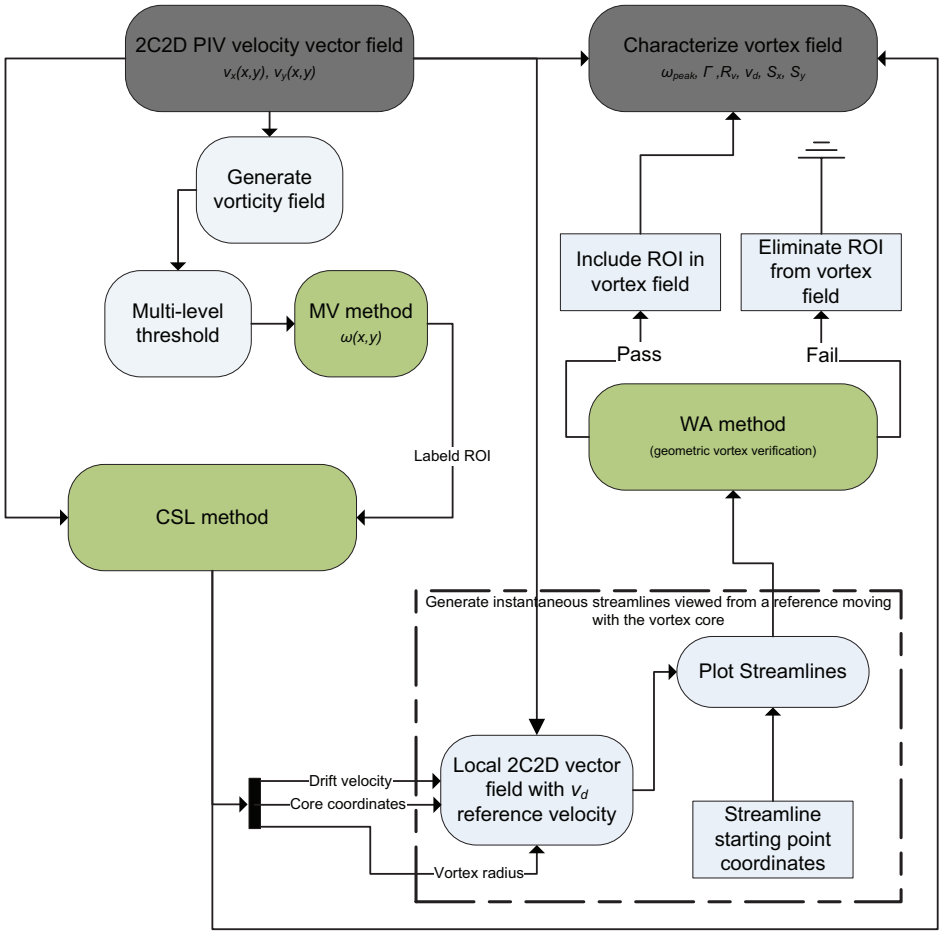

Figure 8:Combinatorial algorithm flow chart

The CVD algorithm is summarized in the flow chart shown in Figure 8. The three individual detection algorithms are displayed as green boxes and the input and outputs (grey boxes) are the 2C2D velocity vector field and the characterized vortex field respectively. The 2D scalar vorticity field is generated from the global velocity map. The vorticity field is indexed by the multilevel threshold algorithm. Combined from with the MV technique, sensible ROI are generated and labeled. The CSL method evaluates each ROI individually and outputs coordinates for the vortex core, the boundary radius and the drift velocity. It is important to remember that the CSL algorithm will report these vortex parameters regardless of a vortex being present emphasizing the CSL method's inability to determine if a vortex exists within a given ROI. This short coming suggests a third algorithm be used to validate the presence of a vortex in a ROI. The WA method can achieve this by searching each individual ROI for closed streamlines and automatically confirm or deny the presence of one or multiple vortices. To be consistent with the definition given by Robinson (1991), the WA method requires instantaneous streamlines computed from a reference frame traveling with the vortex core [8]. This implies that there must be *a priori* knowledge of the vortex, specifically its core coordinates and drift velocity. This is particularly challenging since unlike CSL and MV, WA cannot be performed on the global coordinate system. Instead, local velocity vector maps must be generated for each ROI where the drift velocity, calculated from CSL is subtracted prior to

computing the streamlines. Finally, the WA method either accepts an ROI and labels it as a vortex, or it rejects it.

Experimental Method

An experiment was conducted to capture the velocity flow field immediately downstream from a flapping NACA 0012 airfoil on which the CVD approach was used to identify and characterize vortical structures. The experimental facility consisted of a 0.7x0.4 m (27.5”x16”) water channel with low turbulence characteristics [21]. The airfoil was suspended vertically such that it hangs down through the free surface into the water channel, perpendicular to the upstream flow direction. The experimental PIV setup is illustrated in Figure 10 and consists of four 2112 x 2072 pixel resolution, 14-bit duel-frame CCD cameras (Imager Pro X 4M, LaVision) viewing the investigation plane through 4 independent local coordinate systems. Cameras are calibrated with a 300mm x 800mm calibration target having 1.3mm diameter markers spaced every 3mm. The images are de-warped according to the calibration scales, in order to account for different camera viewing angles and are stitched together with specified offsets to produce one global field. An acrylic sheet was place on the free surface and cameras imaged through it to remove surface refraction effects. A double-pulse Nd:YAG laser (Solo III-15z, New Wave) illuminated the flow which is seeded with 18μm hollow glass spheres (Sphericel, Potters Industries). The laser beam is focused into a thin sheet which is directed upstream by a mirror and submerged periscope. Images were processed through to velocity vectors using commercial software (DaVis 8.0.5, LaVision).

The aluminum airfoil was constructed from a continuous extrusion with a cross-sectional shape of a NACA 0012 airfoil with a chord length C = 75mm. This was suspended on a solid shaft driven by a stepper motor (PK258-02Dl, Oriental Motor) that passes through the airfoil’s aerodynamic center allowing for controlled pitch oscillations of any wave form. A real-time control system written in custom software (DS1104, dSPACE) controlled the stepper motor motion and provided output trigger signals when the airfoil pitch met a desired angle. In this manner, the imaging system can reliably collect data at prescribed positions allowing for both phase averaged and time averaged data sets.

The CVD approach was used to identify and characterize the vortical structures present. The airfoil dimensions as well as parameters describing its motion are shown in Figure 9.

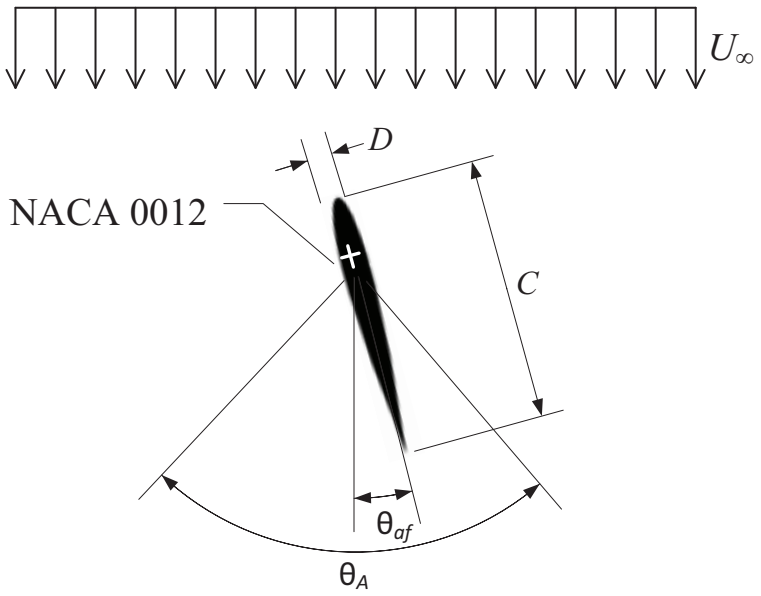

Figure 9: Airfoil dimensions and parameters characterizing its motion

The airfoil of chord length C was limited to small pitch oscillation amplitudes ($\theta_A \leq 8^o$) to prevent the creation of leading edge vortices, which would appear in the wake. A Reynolds number can be defined in terms of airfoil chord thickness D to characterize the flow as:

$$Re = \frac{U_\infty D}{\nu} \tag{17}$$

where for the experiments performed in this study, the free stream velocity U_∞ is held constant at 17mm/s with an airfoil thickness of $D = 8.6$ mm and kinematic viscosity of water is 1×10^{-6} m^2/s so that $Re = 146$. The oscillation waveform is described by $\theta_{af}(t) = (\theta_A/2)\sin(2\pi f)$ and several wake conditions are achieved by changing the oscillation amplitude θ_A and frequency f.

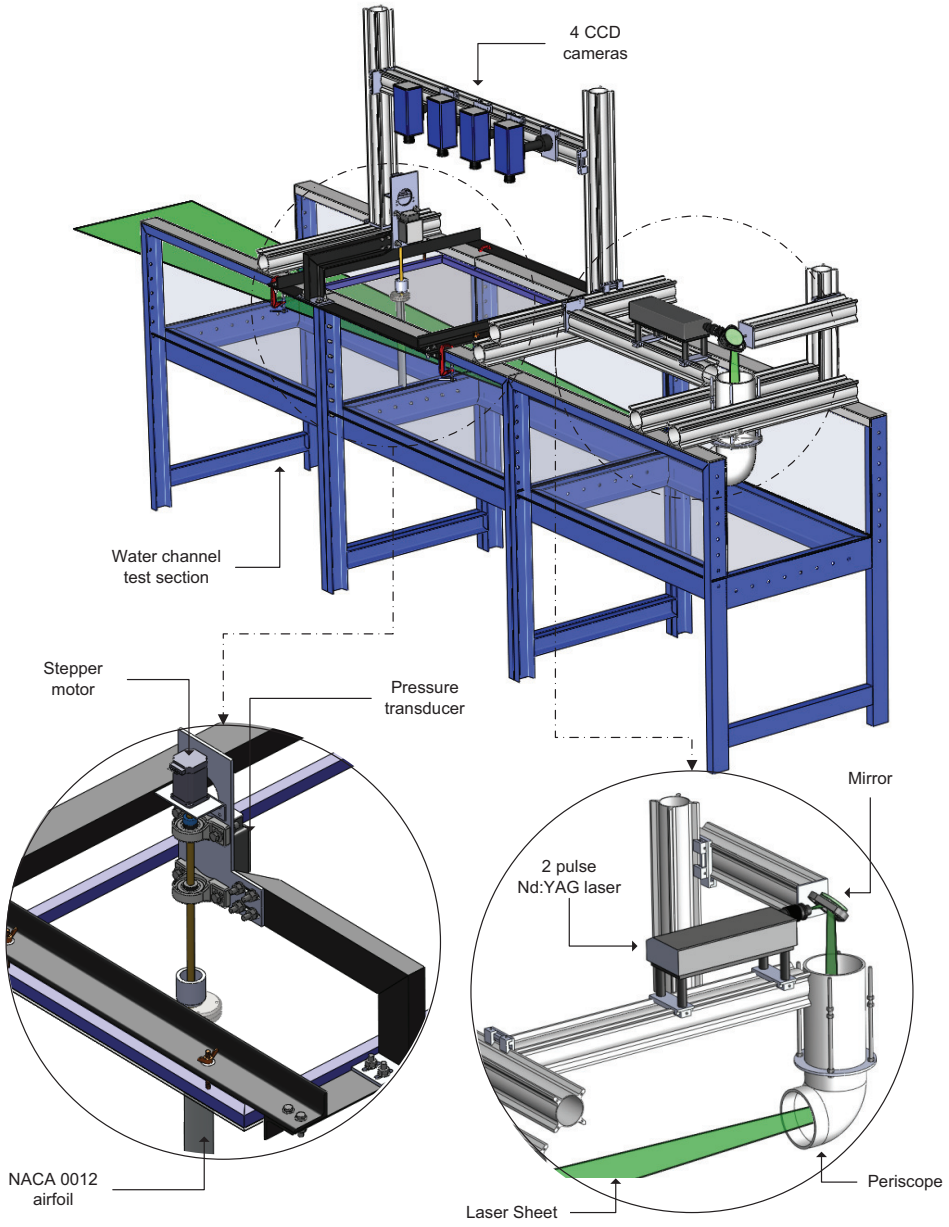

Figure 10:Schematic of the working section of the re-circulating water channel with the PIV experimental setup

Results

A schematic of the oscillating airfoil and its wake is illustrated in Figure 11 and shows the airfoil in relation to generated vortices. Small airfoil oscillation amplitudes allow for an orderly wake with precisely two counter rotating vortices shed per oscillation cycle [2]. The airfoil of chord length C is shown along with the uniform flow of velocity U_∞. The vortices are arranged into two distinct rows which are aligned with the flow and separated by distance S_y. Similarly, the vortices on a given row are separated by S_x. Vortex core coordinates are labeled and a core boundary radius r_v is defined. The drift velocity $\vec{v}_{drift} = (v_{drift,x}, v_{drift,y})$ is the instantaneous velocity vector at the grid point coinciding with the vortex core. The vortices are also characterized by means of peak vorticity ω_{peak} and circulation Γ. Here, the circulation is calculated by summing the vorticity at each velocity measurement location determined by PIV within the radius r_v of a vortex as:

$$\Gamma = \iint_s \left(\vec{\nabla}\times\vec{v}\right) ds = A_{pixel} \sum_{i=1}^{N_i} \sum_{j=1}^{N_j} \omega_{i,j} \qquad (1)$$

Here s refers to the surface integral over area ds and A_{pixel} is the surface area of a rectangle formed from the coordinates of 4 adjacent velocity vectors.

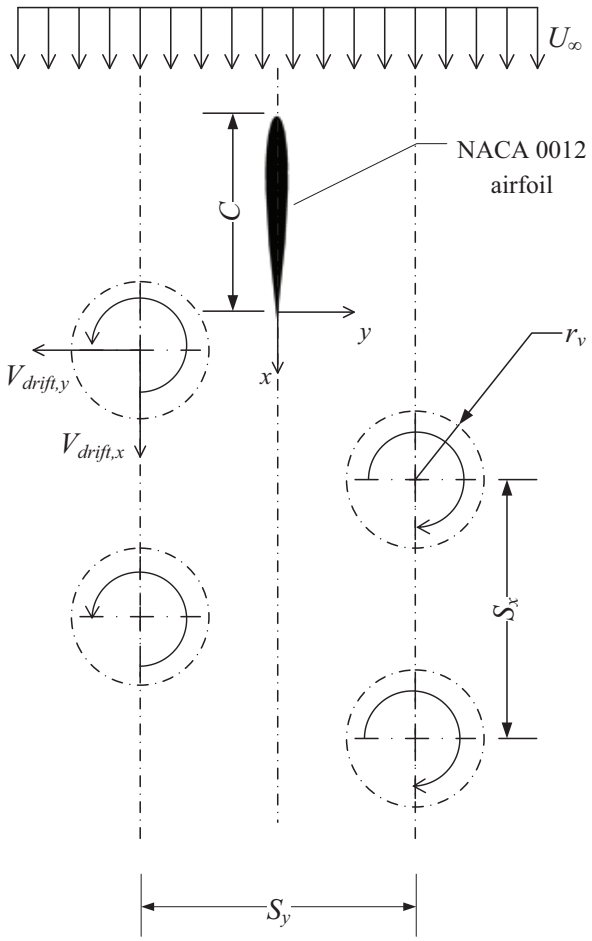

Figure 11:Airfoil wake schematic

By varying θ_A and f, it is possible to achieve different wake arrangements. Common wake

schemes for sinusoidal pitching symmetric airfoils are von Karman, as is shown in Figure 11 which is typical for vortex shedding from a cylinder; aligned, where the transverse separation distance S_y approaches zero; and an inverted von Karman is when the sign of rotation for each row is inverted when compared to the von Karman wake [7].

Instantaneous velocity vector fields are computed for 100 wake data sets collected at an airfoil pitch of 0°. These fields are averaged to produce a single phase averaged. The WA and CSL methods are performed for the 2 phase averaged fields and in Figure 12, the vortex cores and vortex boundary radii obtained from the CSL method plotted over the vorticity field as white crosses and black circles respectively. In order to show the weak vortices clearly, the color map saturates at $|\omega| = 0.8\ \mathrm{s}^{-1}$ in Figure 12 (a) and at $|\omega| = 1.6\ \mathrm{s}^{-1}$ in Figure 12 (b). The von Karman wake shown in Figure 12(a) is the result of sinusoidal pitching at $f = 1.6\ \mathrm{rad/s}$ and $\theta_A = 8°$, and the inverted von Karman wake in Figure 12(b) is the result of sinusoidal pitching at $f = 3.4\ \mathrm{rad/s}$ and $\theta_A = 8°$. These two wakes at $Re = 146$ illustrate the extreme cases of wake vorticity for $\theta_A = 8°$.

The von Karman wake generally produces weak vortices with low peak vorticity and circulation. It exhibits the least vortex decay as a function of downstream distance and has larger stream wise spacing S_x. In comparison, vortices from the inverted von Karman wake have the highest peak vorticity and circulation. They have the highest vortex decay rate and they have relatively small stream wise spacing S_x. These two wake conditions are used as test cases to assess the CVD algorithm's ability to detect and characterize vortices over the range of flow conditions expected in this current low Reynolds number flow ($Re < 200$).

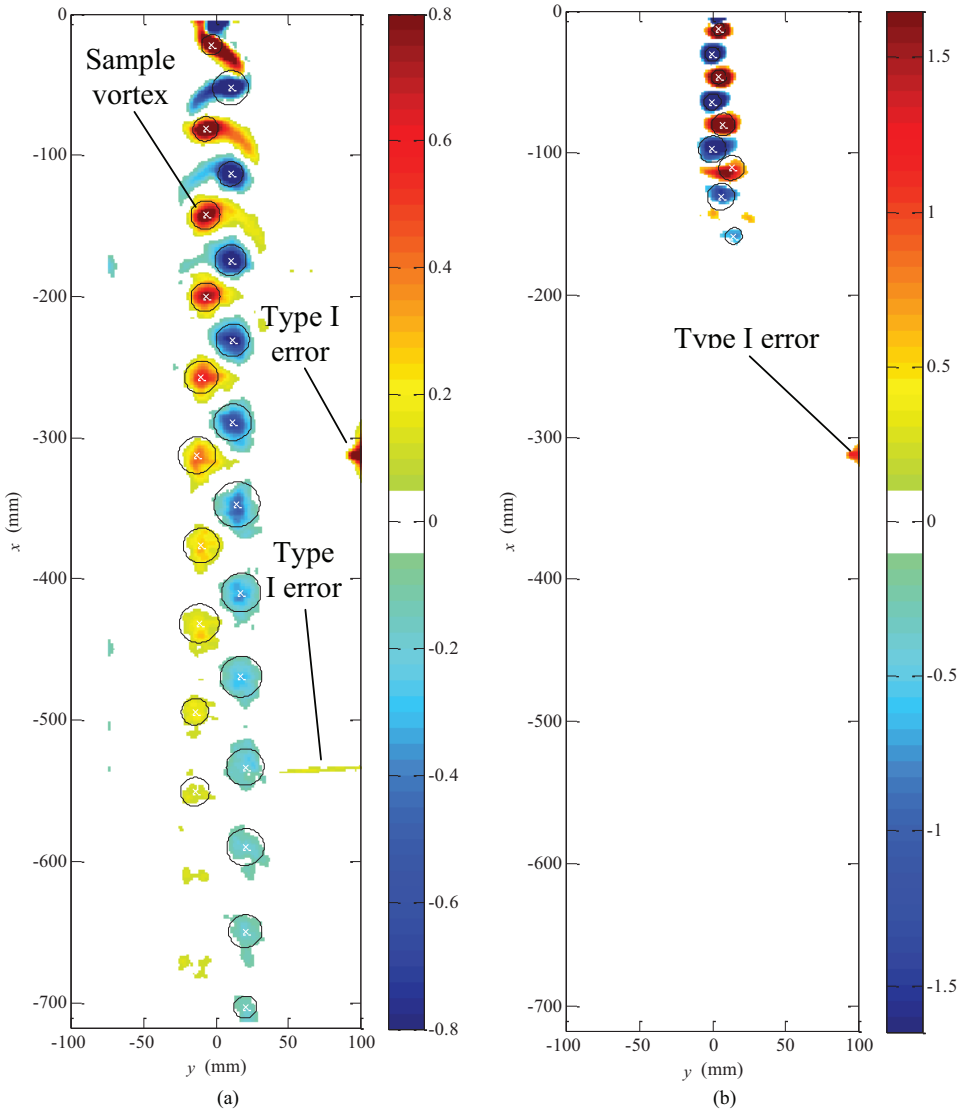

Figure 12:Vortex cores (white '×') and radius (black circles) as computed with the WA and CSL algorithms plotted over the global vorticity map for $Re = 146$ a) $f = 1.6$ rad/s, $\theta_A = 8°$ b) and $f = 3.4$ rad/s, $\theta_A = 8°$.

2.5 WA: to detect errors in WA and CSL

A false positive vortex diagnostic, or a type I error, occurs when an algorithm identifies a vortex that does not truly exist [9], be it due to local shear flow, boundary effects or image stitching errors. Two examples type I errors are annotated in Figure 12 thereby demonstrating the CSL method's inherent inability to reject a ROI which does not enclose a vortex. Once the data from the CSL algorithm is run through the WA algorithm, the false positive is rejected since its streamlines do not form semi-closed, semi-elliptic paths.

A sample vortex is labeled in Figure 12. A local velocity field, centered on the sample vortex core with a moving reference frame equal to the sample vortex's drift velocity as per the pre-WA section of the combinatorial algorithm of Figure 8 is calculated. Figure 13 (a) shows the streamlines that are generated from this velocity field plotted over the local vorticity field. In Figure 13 (b), 5 streamlines meeting the WA requirements are plotted, each complying streamline is mapped to a point (black) along with the vortex core which was previously computed with the CSL method (black '+'). The WA algorithm confirms that the sample ROI contains a vortex that is consistent with the vortex definition of Robinson (1991). It also confirms that only one vortex exists

in the sample ROI and that the core location computed by CSL agrees well with the geometric centre of all the complying streamlines. Should the WA algorithm identify multiple vortices in a single ROI, then the vortex with the largest number of complying streamlines becomes the ROI's primary vortex and the other clusters of streamlines are associated to type II errors.

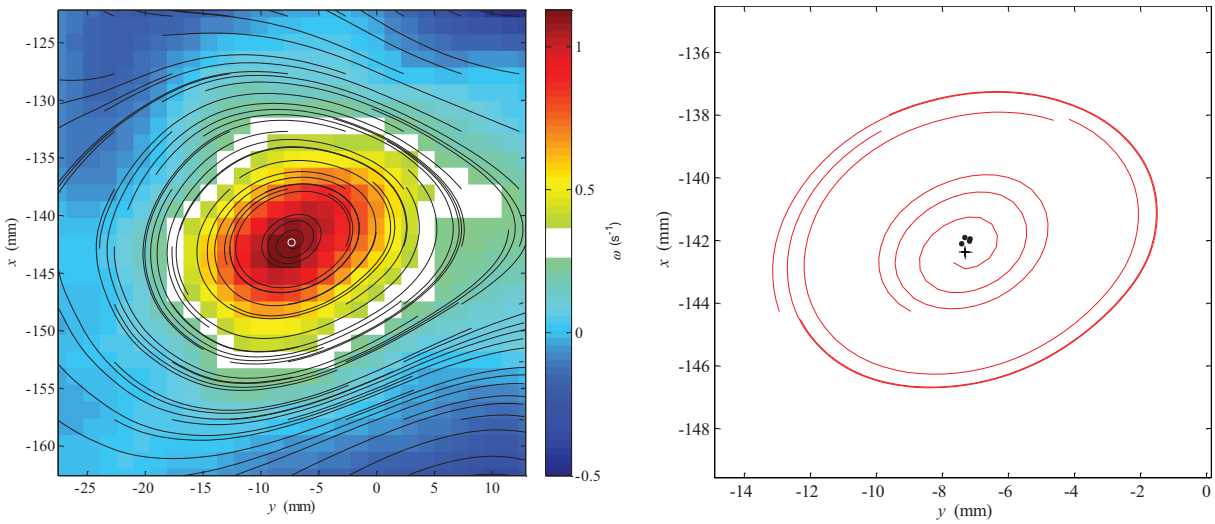

Figure 13 (a)Instantaneous streamlines from the sample vortex's local velocity vector field plotted over the local vorticity map. (b)Complying streamlines as defined by the winding angle algorithm's specifications along with cluster points (black), average cluster point (green point) and vortex core from CSL method (black+)

A false negative, or a type II error, is a vortex which is present in the flow, but goes undetected by the algorithm. Unfortunately, due to the *a priori* knowledge required by the WA algorithm, it cannot avoid type II errors for vortices which are not in the predefined ROI. However, if multiple vortices are in a single ROI, the WA algorithm can identify a type II error, but only if the drift velocity of the false positive vortex is similar to that of the detected vortex. Type II errors for the proposed CVD algorithm may only be minimized through two mechanisms:

1) Wider threshold bounds in the TIV defined in *eqn. 2* for the MV algorithm: Weaker vortices (vortices with low vorticity) are now enclosed by ROI and are consequently considered by the CSL and WA algorithms

2) Smaller sized IM structuring elements in the erosion process: Smaller vortices (vortices with small values of r_v) remain intact during the erosion process and consequently become enclosed by ROI and are considered by the CSL and WA algorithms

Implementing these modifications can cause significant increases in computation time; therefore, defining a minimum vortex size $r_{v,min}$ and strength $\omega_{peak,min}$ prior to running the algorithm is recommended. In doing so, weak and/or small vortices below the threshold are deliberately ignored and the algorithm requires less computation. Both the threshold defined in *eqn. 2* and the sizes of IM structuring element S_{e1}, S_{e2} and S_{e3} are selected on the basis of minimizing type II errors and computation time.

2.6 Vorticity profiles

Vorticity distribution profiles of fully formed vortices are valuable characterization tools. They are useful for evaluating the accuracy of the vortex radius r_v, vortex shape and symmetry and for fitting

analytical models to the vortex under consideration. Figure 14 shows the vorticity of the sample vortex presented in Figure 13 plotted against the dimensionless radius $(y - y_c)/r_v$ along a line of constant y passing through the vortex core. The vorticity profile suggests a Gaussian distribution with slight asymmetry, perhaps due to some interaction with the nearby counter rotating vortex.

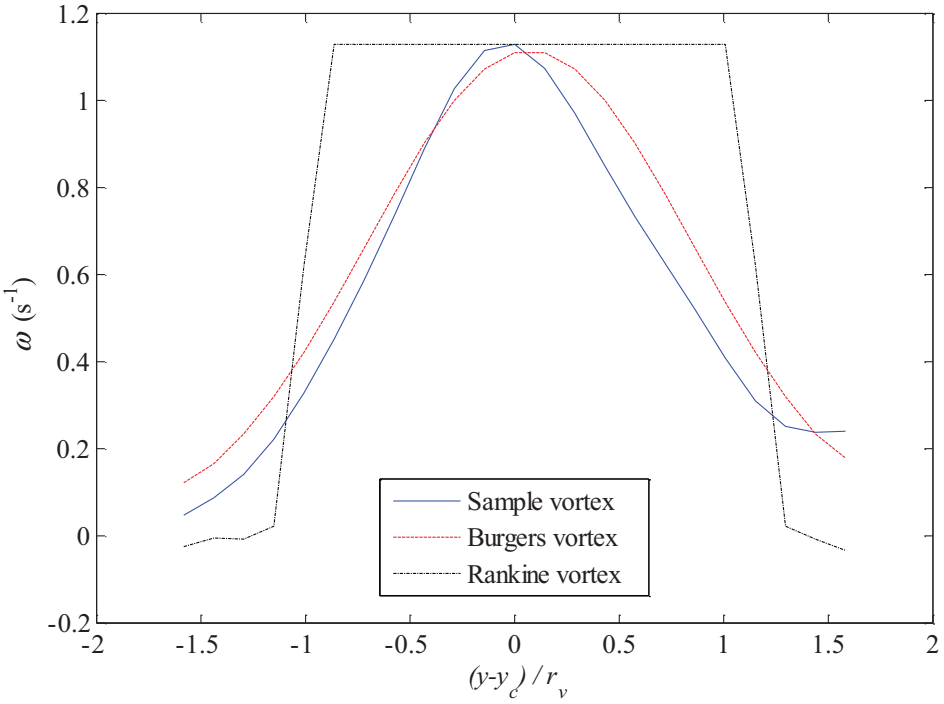

Figure 14: Vorticity vs. the dimensionless vortex radius for the sample vortex, an ideal Burgers vortex and ideal Rankine vortex

Also plotted in Figure 14 are the vorticity profiles for an ideal Burgers and Rankine vortices having the same peak vorticity and radii as those computed by CSL. The Rankine vortex is a simple model which attempts to simulate a real vortex by separating it into two regions, namely the inner core region and the outer core region. Vorticity in the core region is uniform and resembles a forced vortex while the outer core region is free of vorticity thus simulating an irrotational or free vortex [22].

The Burgers vortex solution is a more complicated vortex model often used to illustrate important elements of modern turbulence theory [23]. The Burgers vortex represents an exact solution to the cylindrical Navier-Stokes equations where flow on a cylindrical vortex core inducing a circulation Γ_∞ at large distances is modeled [24]. The circumferential velocity v_θ and vorticity distribution ω of an axisymmetric Burgers vortex in a fluid with kinematic viscosity ν and radius r_v is [25]:

$$v_\theta(r) = \frac{\Gamma_\infty}{2\pi r}\left(1 - e^{-\frac{\gamma r^2}{4\nu}}\right) \tag{18}$$

and

$$\omega(r) = \frac{\gamma\Gamma_\infty}{4\pi\nu}\left(e^{-\frac{\gamma r^2}{4\nu}}\right) \tag{19}$$

Here, γ describes the axial strain $\partial w/\partial z$ in a velocity field $\vec{u}$ described by an irrotational, pure strain, component $\vec{u}_s = (\alpha x, \beta y, \gamma z)$ and a rotational component confined to the xy plane $\vec{u}_w = (u_x, u_y, 0)$. For the case of an axisymmetric Burgers vortex $\gamma > 0$ and $\beta = \alpha = -\gamma/2$

[25].

The vorticity distribution plot in Figure 14 reveals that the sample vortex closely resembles a Burgers vortex having the same radius and peak vorticity as the values computed by the CSL algorithm. This is validation that the CSL algorithm can effectively predict the radius and core coordinates of a vortex from a PIV generated velocity vector field. There is a slight spatial offset between the experimental vortex and the Burgers vortex. This is the result of the CSL algorithm which reads $v_{p(\varsigma,\psi)}$ from *eqn. 5* sequentially from left to right. If the true core coordinate is between two velocity vectors, the algorithm will always chose the leftmost value.

2.7 Circumferential velocity profiles

In addition to vorticity profiles, circumferential velocity profiles prove to be equally useful for characterizing vortical flow structures. Circumferential, or azimuthal velocity is the component of velocity that is perpendicular to any straight line passing through the vortex core. Figure 15 compares circumferential velocity profiles of the sample vortex, a Rankine vortex and a Burgers vortex.

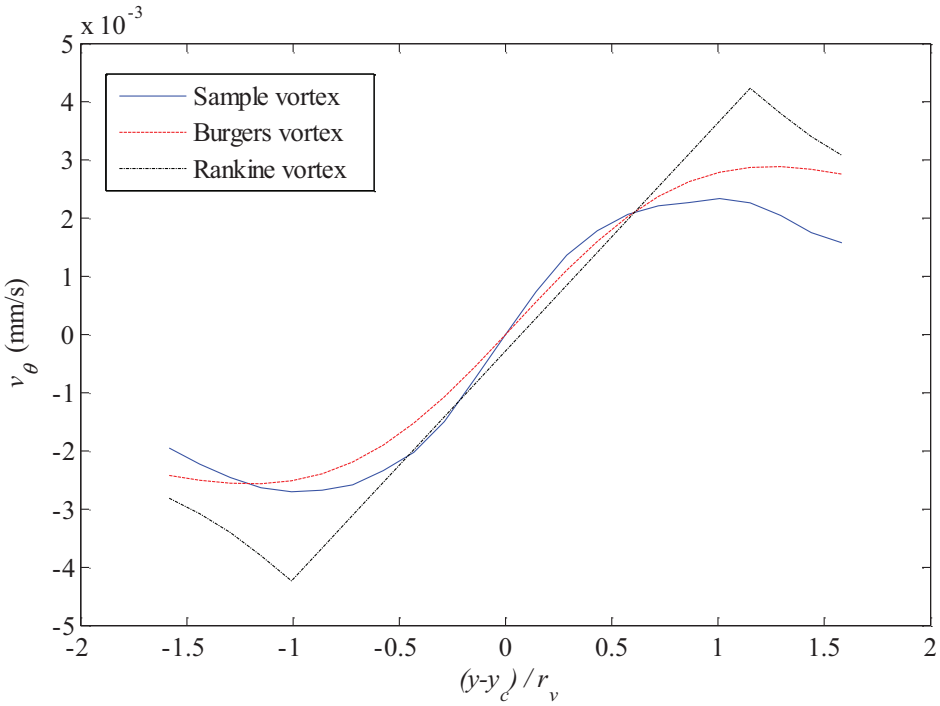

Figure 15: Relative circumferential velocity vs. the dimensionless vortex radius for the sample vortex, an ideal Burgers vortex and ideal Rankine vortex

Figure 15 shows that the sample vortex curve resembles a combination of the Burgers vortex and the Rankine vortex. It can be observed in Figure 14 that defining a vortex boundary radius with a vorticity profile, essentially with the MV method alone, requires an arbitrary cutoff [1]. However, within a vortex radius, the circumferential velocity magnitude is believed to increase with increasing radius and reach a maximum precisely at the vortex boundary r_v [1]. This observation is clearly visible in Figure 15 and it highlights a significant advantage in using circumferential velocity profiles to define vortex boundaries. In addition, locating a vortex core in this manner does not require computation of parameters at or even near the core itself. Rather, it infers the location of the core based on velocity measurements taken at the outer boundaries of the core, where the gradients are much lower. Circumferential velocity profiles demonstrate how the

CSL algorithm can clearly identify the boundary of a vortex core as the radial location of maximum absolute circumferential velocity. This definition of core boundary radius is less ambiguous than one derived from vorticity profiles and hence serves as a superior method for computing vortex boundary radii.

3. Conclusions

A vortex detection and characterization algorithm is developed and tested on 2C2D velocity vector fields taken from the wake of an oscillating NACA 0012 airfoil in a uniform flow. Vortex detection for experimental data is particularly challenging since it is often accompanied by measurement uncertainty and noise [11]. Also, substantial gradients are present near the centre of the vortex often leading to seeding and correlation issues [8]. The algorithm overcomes these limitations in the data sets by making use of three separate detection methods to provide dependable vortex detection for the von Karman and inverted von Karman wakes. The algorithm makes use of the CSL method for characterizing the vortex's core coordinates, boundary radius and drift velocity. The Burgers vortex model most closely matches the vortical structures for this flow so it can be used as a basis for validating the experimental vortex decay results. Vorticity and circumferential velocity profile plots were used to evaluate the CSL algorithm's ability to accurately locate a vortex core, to define the vortex boundary radius and to compute the vortex drift velocity vector. The WA algorithm proved to be a useful verification method for reliably identifying and subsequently eliminating false positives.

Future improvements to the CVD algorithm include development of a more advanced and automated method for tuning threshold intensity vectors *TIV* and for the image morphology parameters. In addition, the CSL method could supply the CVD with a second choice for the core coordinates. In the event that the ROI is rejected by the WA algorithm, the second choice could be used. These modifications aim to reduce true negatives and improve accuracy while minimizing computation time. Finally, a statistical assessment of the combinatorial algorithm's accuracy and repeatability could be compared with those of the individual algorithms to further understand the advantages of using a combinatorial detection approach with experimental PIV data.

References

[1] J. Jeong and F. Hussain, "On the identification of a vortex," *Journal of Fluid Mechanics*, vol. 285, no. –1, p. 69, Apr. 2006.

[2] D. G. Bohl and M. M. Koochesfahani, *MTV measurements of the vortical field in the wake of an airfoil oscillating at high reduced frequency*, vol. 620. 2009, p. 63.

[3] T. Schnipper, A. Andersen, and T. Bohr, "Vortex wakes of a flapping foil," *Journal of Fluid Mechanics*, vol. 633, p. 411, Aug. 2009.

[4] S. Sarkar and K. Venkatraman, "Numerical simulation of thrust generating flow past a pitching airfoil," *Computers & Fluids*, vol. 35, no. 1, pp. 16-42, Jan. 2006.

[5] J. P. Gostelow, M. F. Platzer, and W. E. Carscallen, "On Vortex Formation in the Wake Flows of Transonic Turbine Blades and Oscillating Airfoils," *Journal of Turbomachinery*, vol. 128, no. 3, p. 528, 2006.

[6] J. C. S. Lai and M. F. Platzer, "Jet Characteristics of a Plunging Airfoil," *AIAA Journal*, vol. 37, no. 12, pp. 1529-1537, Dec. 1999.

[7] R. Godoy-Diana, C. Marais, J.-L. Aider, and J. E. Wesfreid, "A model for the symmetry breaking of the reverse Bénard–von Kármán vortex street produced by a flapping foil," *Journal of Fluid Mechanics*, vol. 622, p. 23, Feb. 2009.

[8] H. Vollmers, "Detection of vortices and quantitative evaluation of their main parameters from experimental velocity data," *MEASUREMENT SCIENCE AND TECHNOLOGY*, vol. 12, pp. 1199-1207, 2001.
[9] M. Jiang, "Detection and Visualization of Vortices," Ohio State University, 2002.
[10] S. K. Robinson, "Coherent Motions in the Turbulent Boundary Layer," *Annual Review of Fluid Mechanics*, vol. 23, no. 1, pp. 601-639, Jan. 1991.
[11] N. Saikrishnan, I. Marusic, and E. K. Longmire, "Assessment of dual plane PIV measurements in wall turbulence using DNS data," *Experiments in Fluids*, vol. 41, no. 2, pp. 265-278, Jun. 2006.
[12] P. Moin and K. Mahesh, "Direct Numerical Simulation : A Tool in Turbulence Research," 1998.
[13] H. J. Lugt, "The Dilemma of Defining a Vortex," in *Recent Developments in Theoretical and Experimental Fluid Mechanics*, U. Müller, K. G. Riesner, and B. Schmidt, Eds. Springer, 1979, pp. 309-321.
[14] I. Ari Sadarjoen, "Detection, quantification, and tracking of vortices using streamline geometry," *Computers* , vol. 24, no. 3, pp. 333-341, Jun. 2000.
[15] R. C. Strawn, N. D. Kenwright, and J. Ahmad, "Computer Visualization of Vortex Wake Systems," *AIAA*, vol. 37(4), pp. 511–512, 1999.
[16] L. M. Portela, "Identification and characterization of vortices in the turbulent boundary layer," Stanford University, 1999.
[17] H. Vollmers, "Detection of vortices and quantitative evaluation of their main parameters from," vol. 1199, 2001.
[18] H.-G. Pagendarm, B. Henne, and M. Rutten, "Detecting vortical phenomena in vector data by medium-scale correlation," *Proceedings Visualization '99 (Cat. No.99CB37067)*, pp. 409-552, 1999.
[19] A. E. Perry and M. S. Chong, "Interpretation of flow visualization," in *Flow Visualization: Techniques and Examples*, 1996, pp. 1-26.
[20] I. A. Sadarjoen and F. H. Post, "Geometric Methods for Vortex Extraction," *America*, 1999.
[21] T.L. Hilderman, "Measurement, modelling, and stochastic simulation of concentration fluctuations in a shear flow," University of Alberta, 2004.
[22] D. B. Giaiotti and F. Stel, "The Rankine Vortex Model," University of Trieste, 2006.
[23] J. Gibbon, "Dynamically stretched vortices as solutions of the 3D Navier–Stokes equations," *Physica D: Nonlinear Phenomena*, vol. 132, no. 4, pp. 497-510, Aug. 1999.
[24] P. G. Drazin and N. Riley, *The Navier-Stokes Equations: a classification of flows and exact solutions*. Cambridge University Press, 2006.
[25] A. Prochazka and D. I. Pullin, "Structure and stability of non-symmetric Burgers vortices," *Journal of Fluid Mechanics*, vol. 363, pp. 199-228, May 1998.